# Chapter 43
# Pearce Element Ratio Diagrams and Cumulate Rocks


**J. Nicholls**

**Abstract** While this chapter is about Pearce element ratios, I've included some personal reflections as this book is a 50th Anniversary project of the IAMG. Pearce element ratios, Felix Chayes and the Chayes medal, came together on September 11, 2001. As the recipient of the Chayes Medal, I was in Cancún, Mexico on that fateful date to deliver a talk on Pearce element ratios. Pearce element ratios are designed to model processes of fractionation and accumulation in igneous systems. They are frequently used to extract information from analyses of rocks formed from melts produced by fractionation—volcanic suites. Rock bodies formed from the fractionated crystals—the cumulate rocks—have received practically no attention. From the standard paradigm describing the formation of cumulate rocks, based on studies of the Skaergaard Intrusion, one expects a predicted pattern of data points on a Pearce element ratio diagram. Points derived from the mean compositions of the units in the cumulate body should fall up-slope from the point representing the initial melt composition on a diagram that accounts for the cumulate assemblage. Points derived from the compositions of the inferred residual melts present at the beginning of crystallization of a unit in the rock body should fall down-slope from the point representing the initial magma. The distance between a point on the line of a Pearce element ratio diagram and the point representing the initial magma composition depends on (1) the size of the aliquot that crystallized to form the rock unit and (2) the ratio of crystals to melt in the mush that solidified to form the rock unit. Patterns extracted from computer simulations compared to analogous data points from units of the Skaergaard Intrusion indicate that the crystal mushes that formed the units of the Marginal Border Series had a smaller ratio of trapped melt to crystals than did coeval mushes forming the Upper Border Series. Simulation patterns further indicate that the LZa and UZa units of the Layered Series formed from assemblages with larger ratios of melt to crystals than did the respective coeval units, LZa* and UZa*, of the Marginal Border Series.

J. Nicholls (✉)
Department of Geoscience, University of Calgary, Calgary, AB T2N1N4, Canada
e-mail: jim.nicholls@shaw.ca; nichollj@ucalgary.ca



B. S. Daya Sagar et al. (eds.), *Handbook of Mathematical Geosciences*,
https://doi.org/10.1007/978-3-319-78999-6_43

**Keywords** Pearce element ratios · Cumulate rocks · Computer simulation
Skaergaard intrusion

## 43.1 Introduction

Blue skies and balmy temperatures graced a tranquil world when I entered the lecture room of the hotel-conference center in Cancún, Mexico, venue of the 2001 International Association for Mathematical Geosciences (IAMG) meeting. It was an early Tuesday morning and I was on my way to ensure the equipment worked for the talk I was soon to deliver. I was looking forward to the day and feeling honoured as the recipient of the IAMG Felix Chayes Prize for Excellence in Research in Mathematical Petrology.

When the talk was over and people were thinking ahead to the coffee break and upcoming lectures, we left the lecture room. Up until that moment, we were unaware that the world had changed: hijackers had crashed murder-suicide planes into the World Trade Center in New York City. Those attending the meeting gathered around a TV and watched the horror of the south tower collapse; smoke and dust billowed down the streets of New York, chasing people as they ran for their lives. The north tower collapsed a few minutes later. Hijackers crashed another plane into the Pentagon, and a fourth had been brought down in a field in near Shanksville, Pennsylvania just minutes away from its target in Washington, D.C. It was September 11, 2001, referred to by nearly all as 9/11.

My talk on Pearce element ratio diagrams and their utility in evaluating petrologic hypotheses was largely forgotten, understandably, in the turmoil following the events of that morning. Pearce element ratios and the events of 9/11 have been inextricably linked in my mind since that terrible morning, which is why they come together in this chapter.

Pearce element ratios were conceived in the last century (Pearce 1968), as were the concepts and techniques needed to implement their application. Their defining characteristic is a denominator formed from concentrations of elements that enter the minerals crystallizing from igneous melts in negligible amounts. Pearce element ratios have been used to model the evolution of melts in volcanic systems (see Nicholls and Russell 2016 for recent applications and explanations of the concepts) but they have not seen much service in modeling changes in the concomitant rocks formed from the separated solids and the enclosed interstitial melts: the cumulate rocks. Pearce element ratios can provide insight into the evolution of such assemblages.

## 43.2 Outline of a Cumulate Rock Paradigm

Petrologists have developed a paradigm for the crystallization of a single magma body in a crustal magma chamber that explains many of the features of layered and cumulate igneous rocks. This paradigm originated in features found in the Skaergaard Intrusion of East Greenland (Wager and Deer 1939; Carmichael et al. 1974; McBirney 1989a, 1996).

Cumulate bodies are often huge; the Bushveld Complex in South Africa has an estimated volume between 370,000 and 1,000,000 $km^3$ (Cawthorn and Walvraven 1998). Each unit forms by crystallization of a portion or aliquot of the melt in the magma chamber at the time. The larger the unit, the larger the aliquot from which it formed.

A cumulate body can be enclosed by a shell of finer grained rock petrologists are wont to call a chilled margin. The standard inference is that the chilled margin represents the initial magma and that the composition of the chilled margin closely approximates the composition of the initial magma. However, the chilled margin of a large body can be a boundary layer formed by the reaction of the corrosive magma with the country rocks. If so, the composition of the chilled margin can differ from that of the initial magma in a way that depends on the composition of the country rock and on the extent of reaction between magma and country rock. Nevertheless, chilled margins need to be considered as possible samples of the initial magma.

### *43.2.1 The Skaergaard Intrusion*

The Skaergaard Intrusion in East Greenland is one of the most studied rock bodies on the face of the Earth. L.R. Wager discovered the intrusion in 1931 on a scientific expedition. He returned in 1932 on another expedition and again in 1935–36 when he organized and led the third expedition to map and study the intrusion. On this trip, W.A. Deer accompanied him. Publications on the petrology of the Skaergaard began with the report by Wager and Deer (1939). A facsimile of the report was issued in 1952 with a new preface and a list of papers published since the 1939 publication. The list contains 46 references. One can find several hundred references that target the Skaergaard in the literature published after 1952.

I never met Wager but I did meet Deer when he visited the University of California, Berkeley during my time there as a graduate student. On a field trip, he spoke briefly about working with Wager on the Skaergaard. Wager was a mountaineer and climber. In 1933, as a member of the British Expedition to Mount Everest, he climbed to more than 8595 m, setting a record for a climb without oxygen, a record that wasn't bested until 1978. It the preface to the original report, Wager and Deer wrote that the terrain was so demanding that the two-man mapping parties had to traverse roped together, which lends credence to the story in which

Deer was reputed to have said he woke scared nearly every day on the Skaergaard because Wager took them up and down cliffs and slopes where Deer would never go himself.

Significant contributions to Skaergaard petrology since the original Wager and Deer report in 1939 have come from Wager (1960), Wager and Brown (1968), Hoover (1989a, b), McBirney (1989a, b, 1996), Ariskin (2002), and Nielsen (2004) among many others. As a result, the Skaergaard Intrusion has become a standard of comparison against which the evolutionary paths of basaltic magmas are measured.

The major units of the intrusion are the Layered Series (LS), composed of relatively horizontal layers, the Marginal Border Series (MBS) composed of relatively steeply dipping layered rocks, and the Upper Border Series (UBS), composed, again, of relatively horizontal layers of rock (Fig. 43.1). The layers in the Layered Series and the Upper Border Series become approximately horizontal after removal of a post-intrusion tilting (McBirney 1989a). The smaller units, Lower Zone a, Lower Zone b (LZa, LZb), etc. (Fig. 43.1) are defined by mineralogical changes. For example, the coeval units of the Middle Zone (MZ, MZ* and $\beta$) are characterized by the absence of large, primary crystals of olivine (primocrysts) (McBirney 1989a). Olivine primocrysts occur throughout the rest of the intrusion.

The stratigraphic nomenclature has slightly changed with time. Earlier workers, for example, Wager and Deer (1939), Chayes (1970), Carmichael et al. (1974), and

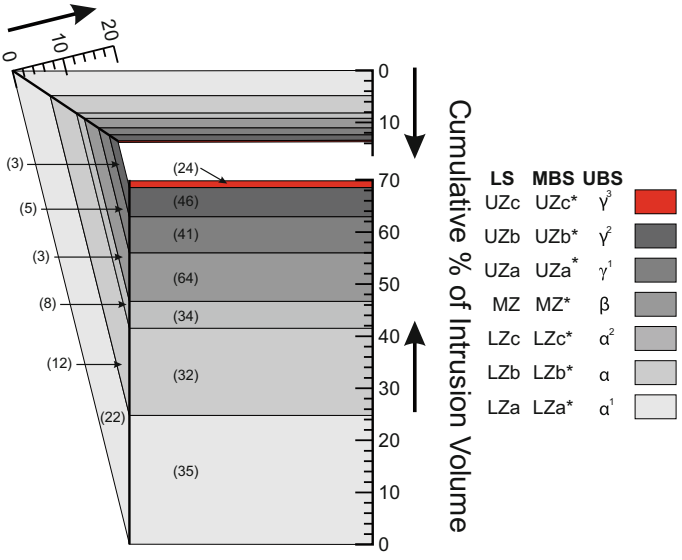


**Fig. 43.1** Rock units of the Skaergaard Intrusion (modified from Nielsen 2004). The Layered Series is interpreted to have formed by sedimentation of the crystallizing minerals onto the floor of the magma chamber. The Marginal Border Series (Hoover 1989a, b) and the Upper Border Series (Naslund 1984) are thought to have formed by plating of the crystallizing minerals on the walls and roof of the magma chamber. Labels in parentheses are number of analyses used to calculate the mean compositions of the rock units (McBirney 1989a)

Naslund (1984) called the Marginal Border Series and Upper Border Series (UBS) the Marginal Border Group and Upper Border Group. In addition, an asterisk has been attached to the names of the units of the Marginal Border Series to distinguish them from the units of the Layered Series.

The original floor of the magma is not exposed so the first rocks that formed on the floor are not available nor are samples from UZc* in the Marginal Border Series because of lack of outcrop (Hoover 1989a). The last or nearly last melt in the chamber is believed to have been caught between the crystal mush of solids and trapped melt that solidified as UZc* and the bottom of the UBS where the youngest unit of the UBS, the $\gamma^3$ unit, crystallized.

According to the paradigm, the rocks making up the intrusion formed by sedimentation of the crystallized minerals on the floor of the chamber and by plating minerals on the roof and walls. The solid assemblages that formed as sediments and as layers of plated minerals change with crystallization stage as do the mineral compositions. These mineral assemblages and mineral compositions found in the bottom, sides and top of the solidified magma chamber can be correlated and a stratigraphy of mineral assemblages and compositions provide coeval markers of crystallization stage. The rocks making up the intrusion consist of the mineral sediments and plated crystals plus melt trapped between the minerals; the trapped liquids later crystallize, creating intercumulus assemblages that, with the primocrysts, make up the rock units that fill the magma chamber.

Properties not emphasized but usually implicit in this paradigm are the ideas that the initial magma filling the magma chamber is uniform in composition and that the compositions of successive melts in the shrinking chamber maintain uniform compositions. These ideas may not be realistic. There may be compositional gradients as well as temperature and pressure gradients in the melt that induce the density currents that develop sedimentary structures, such as cross bedding, in the crystal mush.

In addition, the sedimentation-plating paradigm fails to account for several features of cumulate rocks, for example, repetition of stratigraphic units in the sedimentary layers (Bons et al. 2015). Mush formation above the magma interface (Bons et al. 2015) and double-diffusive convection in boundary layers (Huppert and Turner 1981; McBirney and Noyes 1979; McBirney 1985) are processes postulated to account for the repetition.

Processes behind the magma-mush front (post-cumulus processes, Sparks et al. 1985) can also affect the mineralogy and chemistry of the phases involved in the evolution of the magma body. These processes include convection in the trapped melt, compaction, and cementation. Cementation could produce significant chemical changes in the cumulate rock. Large, optically continuous crystals (poikilitic crystals) can be found enclosing previously formed primocrysts in both lava flows and in cumulate rocks. In the Skaergaard Intrusion and larger cumulate bodies, an interconnected crystal of pyroxene or plagioclase often fill the interstices between the primocrysts.

One infers the primocrysts were originally enclosed in a melt with the same composition as the melt that filled the magma chamber at the time and that melt was

trapped between the primocrysts on the boundaries of the magma chamber. On crystallization of the interstitial melt, a single crystal can grow, fill the interconnected spaces, and displace the trapped melt. The melt, after undergoing post-cumulus processes, will differ in composition from the initially trapped melt. This modified melt could be expelled from the crystal pile and mix with the magma in the chamber, changing its composition. The large poikilitic crystals left behind would be part of the cement that holds the rock together.

Granted that processes in front of and behind the crystallization boundary can affect the resulting cumulate rock, the questions are: how effective are they in changing the rock composition and do they have a detectable influence on the composition of the melt in the chamber?

When the trapped melt crystallizes, permeability decreases, flow of melt from the cumulate mush slows, and its potential to change the composition of the melt in the magma chamber is lowered.

The difference in composition between the trapped melt and the melt in the magma chamber affects the composition of a mix of the two. If the trapped melt differs only slightly from the composition of the melt in the magma chamber, then the composition of a mix will differ from that of the composition of the melt in the magma chamber by a small amount, especially if the amount of trapped melt added to the mix is small.

Melt trapped in the crystal mush close to the crystallization boundary will be close in composition to the melt in the magma chamber. Farther from the boundary, the compositional differences will be larger. However, post-cumulus processes will act to decrease the volume of the trapped melt farther from the boundary. Processes like compaction, adcumulus growth (crystal growth on the surfaces of the primocrysts exposed to the interstitial melt), and cementation.

Expulsion of the trapped melt from the crystal mush could change the chemical composition of the melt in the magma chamber; however, the physical setting and processes could work in concert to keep the changes small.

Magma mixing, magma recharge, and magma mingling are labels for similar if not nearly identical processes. Simply put, the terms label the incorporation of one magma into another. If the invasive magma has a different composition than the original, the final body will have a different composition from the original (Anderson 1976; Carmichael 2004). Again, the effect of mixing on the chemistry of the combined magmas depends on how different the compositions are. The greater the differences, the greater the effect.

## 43.3 Pearce Element Ratio Patterns for Cumulate Rocks

The data to test any model of cumulate rock formation, Pearce element ratio or otherwise, comes from geologic maps, mineralogy, rock and mineral compositions, and rock textures. The more features of the data a model can predict, the stronger the model. If the model conforms to the data, the model is accepted as a description

of the implied process that formed the rocks. If the model does not conform to the data, the model is rejected as an explanation (Nicholls and Russell 2016).

The numerators of the ratios plotted on the rectilinear axes of a Pearce element ratio diagram reflect the chemical changes in the melt-solid system caused by segregation and accumulation (sorting) of a specified mineral assemblage. Specification of the mineral assemblage allows us to create a model such that the compositions of melts and solid assemblages will fall on a line with the model slope. Only one rock composition is needed to locate the model line in Pearce element ratio space. The other analyses in the set of rock analyses can then be used to test the model. The specifics of the model dictate the slope of the line. Usually, the slope is one by design. Consequently, we can talk about up-slope and down-slope directions from a fixed point on the model line. If we select the point representing the chemistry of the melt present when the rock unit begins to form as the fixed point, then a point representing the chemistry of the derivative or residual melt will fall down-slope from the fixed point. Points representing the chemistry of crystal-melt mixtures (crystal mushes) will fall up-slope from the fixed point.

The general pattern expected for data points representing melts from a system undergoing sorting are known (Pearce 1968; Russell and Nicholls 1988; Nicholls and Russell 2016). The details of patterns expected in the data collected from cumulate bodies have not been explicitly investigated. A simple computer simulation of accumulation processes can delineate at least some of the expected patterns. Details of the simulation are described in the appendix.

The results of a simulation for a system with the composition listed in Table 43.1 are shown on Fig. 43.2. The Pearce element ratios plotted on Fig. 43.2 are:

$$(0.8\,\mathrm{Al} + 0.5\,\mathrm{Mg} + 0.4\,\mathrm{Ca})/\mathrm{K}\ \text{versus}\ \mathrm{Si}/\mathrm{K}$$

The diagram was designed to describe the Pearce element ratios in the melts generated by fractionation (loss) of anorthite ($CaAl_2Si_2O_8$) and forsterite ($Mg_2SiO_4$) from the initial melt. The Pearce element ratio coordinates of the initial melt are shown with a black star on Fig. 43.2. The ratios derived from the compositions of the solids plus trapped melt are shown by filled circles.

**Table 43.1** Composition of the melts in the simulated crystallization processes

| Element | Melt 1 | Melt 2 |
|---|---|---|
| Si | 50% | 52% |
| Al | 20% | 19% |
| Mg | 15% | 14% |
| Ca | 10% | 10% |
| K | 3% | 2.5% |
| P | 2% | 2.5% |
| Size | 10000 m units | |
| Aliquot | 25% | |

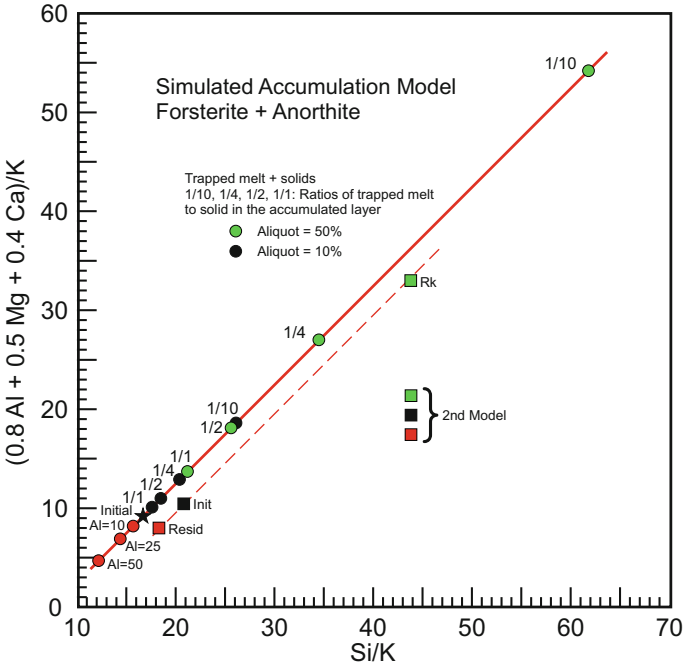


**Fig. 43.2** Pearce element ratio diagram for crystallization of a simulated system containing Si, Al, Mg, Ca, K, and P. Forsterite and anorthite are subtracted from the initial melt, leaving a residual melt that is trapped in the solid assemblage. Rocks formed by the simulated process would be composed of forsterite, anorthite, and solidified trapped melt (see appendix)

As expected, all the data points generated by the simulation fall on a line with a slope of one. The residual melts do produce points on the line that fall down-slope from the point representing the initial melt. Points representing the compositions of the accumulated solids and trapped melt and do plot up-slope from the point representing the initial melt (Fig. 43.2). These relationships are simply examples of the lever rule of phase diagrams (see Bloss 1994, pp. 304–306).

A second model is shown with a dashed line on Fig. 43.2. If the magma chamber undergoes recharge by a similar but not identical magma, we would expect the same ratio pair to describe the variation produced by crystallization of the second melt. The composition of the second simulated melt that produced the data points shown by squares is listed in Table 43.1. Mixing and crystallization of the mixed melts would produce data points falling between the two model-lines.

If the coordinates of the fixed point on a Pearce element ratio diagram are $(x_i, y_i)$, then the distance between the fixed point and another point on the model line with coordinates equal to $(x_j, y_j)$ will be given by:

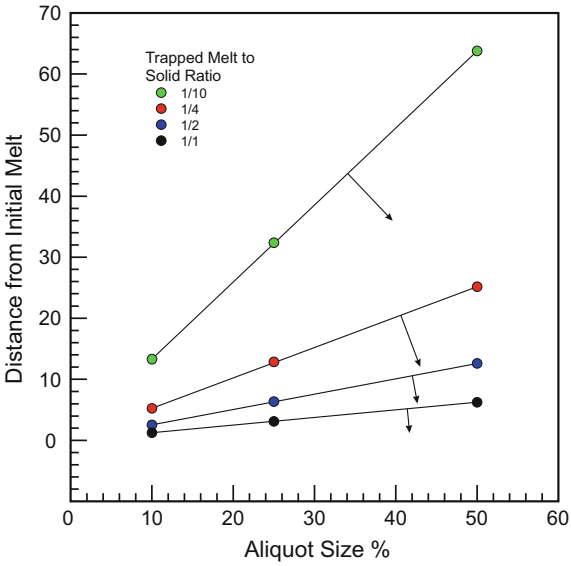


**Fig. 43.3** Plot of distance along the model line with a slope of one (red line in Fig. 43.2) from the point representing the initial melt (star in Fig. 43.2) against aliquot size. The arrows indicate direction of increasing ratio of trapped melt to cumulate solids

$$d = \left(x_i - x_j\right)\sqrt{2}$$

if the slope is equal to one and if the points representing cumulate assemblages fall exactly on the model line.

Two quantities determine the distance of a point from the fixed point: the size of the quantity of melt (aliquot) that crystallized to form the unit of crystals plus trapped melt and the amount of melt trapped in the crystal mush. Figure 43.3 shows how distance along the model line, aliquot size, and ratio of trapped melt to solid are related in the simulated system.

The two variables, distance along the model line and aliquot size, work in concert. The two are also quantities that can be extracted from sets of rock analyses and from geologic maps. The relationship between the two can be described by treating the ratio of the amount of trapped melt to the amount of accumulated crystals in a single unit of the cumulate rock body as a parameter. On a plot of aliquot size versus distance from the point representing the melt along the model line, lines of constant ratio of trapped melt to solid in the mush fan across the diagram. The smaller the ratio, the farther the line of constant ratio falls from the x-axis (Fig. 43.3).

Approximations of the amount of trapped melt could be made from estimates of petrographic modes (Chayes 1956; Nicholls and Stout 1986) of intercumulus assemblages versus primocrysts in thin section. However, distinguishing adcumulus growth from original growth material of the primocrysts is sometimes difficult. In addition, modal variations must underlie the large chemical variations found in the units of cumulate rocks (see below, Sect. 43.4). Consequently, petrographic assessment of the ratio of the volumes of trapped melt to primocrysts would require

looking at many samples to get a precise value for a unit in the intrusion. At the present time, data to make a quantitative assessment of the agreement between model values and precise estimates of the petrographic modes are not available.

## 43.4 Compositions of Units of the Skaergaard Intrusion

A challenge to the construction of viable Pearce element models of cumulate rock formation arises from the chemical and mineralogical heterogeneity in the map units. The compositions of the constituent units must be determined as the mean of analyses from different locations in the unit. Mean values of the compositions and standard deviations for each constituent were published by McBirney (1989a, 1996) with data from Naslund (1984) for the Upper Border Series units. Dividing the standard deviations by the square root of the number of samples gives the standard errors of the means; the accepted measure of the uncertainty in a mean value. Standard errors of the means are large compared to analytical uncertainty (compare McBirney 1989a; Wright et al. 1975, p. 117). Analytical uncertainties are often two orders of magnitude smaller than the standard errors of the means. To make the two measures of uncertainty approximately equal, on the order of 10,000 samples would have to be analyzed for each unit.

When evaluating a model by comparing values from the model with the data, we expect certain criteria to be met if the model is successful. When testing models treating volcanic rocks, we expect model values to agree with the analytical data to within analytical uncertainty (Nicholls and Russell 2016; Nicholls and Stout 1988). Implicit in this expectation is the assumption that a sample from a lava flow is representative of the flow itself.

Estimates of the proportional volumes (Nielsen 2004) are shown on Fig. 43.1. The proportions, expressed as percentages of the volume of the intrusion were derived from the geologic maps of the body. It is worth explicitly noting that the quantitative entity plotted on Fig. 43.1 is volume, not thickness as has been traditionally plotted on similar looking graphs. Distances along the parallel lines have no real-world significance. The proportional volumes shown on Fig. 43.1 are not all independent (Nielsen 2004, p. 519). This dependence is revealed on Fig. 43.1 by the straight lines separating Layered Series volumes from the Marginal Border Series volumes and the Marginal Border Series volumes from the Upper Border Series volumes.

The abundant primocrysts in the intrusion are plagioclase, olivine, pyroxene (high-Ca augite and low-Ca pigeonite since inverted to orthopyroxene), and Fe-Ti oxides. The Middle Zone of the Layered Series, the Middle Zone of the Marginal Border Series, and the Upper Border Series $\beta$-zone lack olivine primocrysts, their place taken by low-Ca pyroxene.

### 43.4.1 Pearce Element Ratios and the Skaergaard Intrusion

We would like a Pearce element ratio design such that the products of sorting of all the mineral-melt assemblages in the intrusion would have compositions that generate points along a straight line with a slope of one. Unfortunately, nature prevents construction of such a diagram. The stoichiometry of olivine, $(Mg, Fe)_2SiO_4$, and low-Ca pyroxene, $(Mg, Fe)_2Si_2O_6$, with their different ratios of (Mg, Fe) to Si lead to an inconsistent set of algebraic equations in the design matrix (Nicholls and Russell 2016; Nicholls and Gordon 1994). We can, however, design two diagrams, one that accounts for sorting of olivine, plagioclase, augite, and Fe-Ti oxide and another that accounts for sorting of low-Ca pyroxene, plagioclase, augite, and Fe-Ti oxide.

Two ratio pairs that account for the abundant phases and their different compositions are:

[0.25 Al + 0.5(Fe + Mg) + 1.5 Ca + 2.75 Na]/K versus
(Si + 1.5 Ti)/K
(Olivine in the sorted assemblage)

and

[0.5 Al + Fe + Mg + Ca + 2.5 Na]/K versus
(Si + 3 Ti)/K
(Low-Ca pyroxene in the sorted assemblage)

Pearce element ratio diagrams for the two ratio pairs appear on Figs. 43.4 and 43.5. Figure 43.4 shows the diagram for olivine in the sorted assemblage whereas Fig. 43.5 shows a diagram for low-Ca pyroxene in the sorted assemblage.

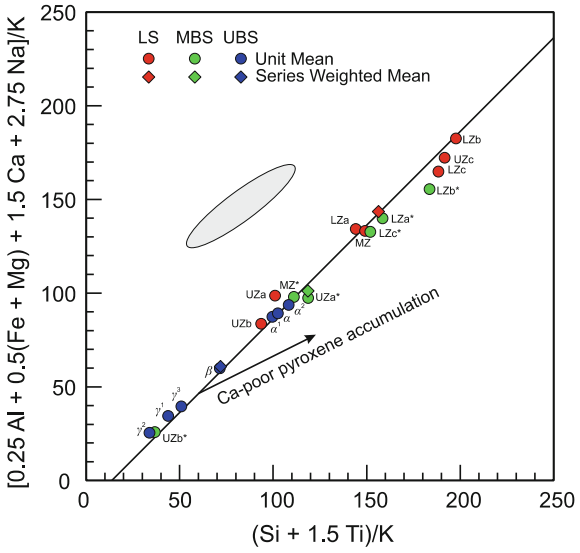


**Fig. 43.4** Pearce element ratio diagram designed to show the effects of sorting plagioclase, augite, olivine, and Fe-Ti oxide ($Usp_{75}$). Accumulation of Ca-poor pyroxene in addition to the listed minerals would cause data points to fall away from the model line along trends parallel to the arrow. The grey ellipse represents the size of the 1σ uncertainty in the location of the data point for UZb*

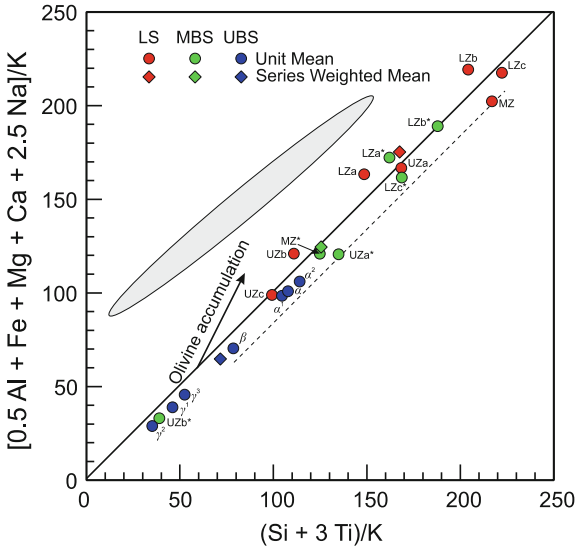


**Fig. 43.5** Pearce element ratio diagram designed to show the effects of sorting plagioclase, augite, Ca-poor pyroxene, and Fe-Ti oxide ($Usp_{75}$). Accumulation of olivine in addition to the listed minerals would cause data points to fall away from the model line along trends parallel to the arrow. The grey ellipse represents the size of the 1σ uncertainty in the location of the data point for UZb*

The points on the diagrams were calculated from the mean values of the compositions (McBirney 1989a, 1996). On both diagrams, the points are distributed along a trend with a slope of one but with considerable scatter; more scatter than found in trends calculated for suites of cogenetic volcanic rocks (compare Figs. 43.4 and 43.5 with diagrams in Nicholls and Russell 1991, 2016). The Skaergaard data span a larger range of values than do data from volcanic suites when plotted on similar Pearce element ratio diagrams. Data collected from basaltic volcanic suites, when plotted on comparable diagrams, span approximately 50 units (see Nicholls and Russell 1991). The Skaergaard data span approximately 250 units.

Although the number of analyses for several of the units in the Skaergaard Intrusion is large enough to make the mean values relatively stable in the sense that one more analysis would have a small effect on the mean, especially if the one analysis were for a rock like the ones analyzed. However, the large standard errors attached to the mean values opens the possibility that analyses of another set of samples of the same size collected from the same unit could result in a different set of means for the constituent oxide values.

Propagating the standard error of the means through the procedure for calculating the uncertainty in the location of a data point (Nicholls 1990b) produces large ellipses of 1σ analytical uncertainty in the location of the data point. The smallest ellipses for the data points shown on Figs. 43.4 and 43.5, belong to the points representing the mean of the UZb* unit of the Marginal Border Series.

The sizes of the uncertainty ellipses render them useless for testing the model. Almost any line with a slope of one will intercept the uncertainty ellipses. The model cannot be rejected because of the scatter of the data points off almost any line with a slope of one that we can pick.

Although the data points on Figs. 43.4 and 43.5 fall along a trend with a slope of one, the scatter about the trend precludes there being an obvious choice for a point through which to draw a model line. We could draw lines with unit slopes through every one of the data points but could not justify picking any one line over the others.

We can, however, calculate the mean compositions of each series (LS, MBS, UBS) by weighting the mean compositions of the units in the series by their respective relative volumes. The points derived from the weighted means are plotted as diamonds on Figs. 43.4 and 43.5. The points representing the weighted means do fall on a trend with a unit slope and with less scatter than do the full set of data points. It is a straight-forward procedure to find a line with a slope of one that falls closest, in the least-squares sense, to the three points representing the weighted mean compositions of the three series that make up the intrusion. The best fit lines for the weighted means fall close to the respective points (Figs. 43.4 and 43.5), well within any $1\sigma$ error ellipse. These lines we will use as our model lines.

The inclusion of olivine or low-Ca pyroxene in the model assemblages produces no statistically significant difference in the efficacy of testing the models that I can see. If the lines defined by the weighted mean compositions for the three Series (LS, MBS, UBS) are the best models, then one would expect the points representing the Middle Zone rocks (MZ, MZ*, $\beta$) on Fig. 43.4 to deviate by falling below the line. They don't fall farther from the line than do points for the other units. Rather, they often fall closer to the line. Possibly, low-Ca pyroxene accumulated in the Middle Zone units in insufficient amounts to be detected with the olivine-sorting model.

On Fig. 43.5, one would expect the points representing the units outside the Middle Zone units to fall above a model line through points representing the Middle Zone rocks. The dashed line on Fig. 43.5 is a best fit line with a slope of one and is defined by the three Middle Zone values (MZ, MZ*, $\beta$). The data points for the other units displayed on Fig. 43.5 are displaced as expected if olivine sorting happened; they fall above the line.

The points representing the units (filled circles) fall in overlapping clusters along a trend with a slope of one with the larger units of the Layered Series generally falling up-slope from the points representing the Marginal Border Series units and with the Upper Border Series points falling farthest down-slope. This distribution is consistent with predictions from the computer simulations. The points representing Series compositions (filled diamonds) are also distributed as predicted by the computer simulation; the larger aliquot plots up-slope and the smaller aliquot down-slope.

The trends followed by the data points on Figs. 43.4 and 43.5 are consistent with the predictions of the models. Given the size of the uncertainties in the locations of the data points, there is no evidence that more than one magma was involved in the formation of the Skaergaard Intrusion.

## 43.5 Melts of the Skaergaard Intrusion

Three categories of melt crystallized to form the Skaergaard Intrusion: the melt that initially filled the magma chamber, the subsequent melts residual to each crystallization stage, and the melts trapped between the primocrysts. Melts trapped in the oldest part of a unit would have a different composition from melts trapped in the youngest part of a unit. Melt trapped in the youngest part of the unit would have the composition of the residual melt at the time of entrapment. Between crystallization of the oldest and youngest crystals in the units, the trapped melt would have compositions gradational between the two.

Any melt that existed in the Skaergaard crystallized long ago. Perforce, estimates of their compositions and their nature must be inferred. Melts whose compositions we can infer are those for the initial melt and the residual melts filling the magma chamber at the end of the formation of each rock unit and the beginning of the next.

### *43.5.1 The Initial Melt*

Pearce element ratios for estimated compositions of the initial melt are plotted on Fig. 43.6. The initial melt composition should plot down slope from the point representing the mean composition of the Layered Series. Estimates of the initial Skaergaard magma have been made by Wager (1960), Hoover (1989a), McBirney (1996), Ariskin (1999), and Nielsen (2004). Wager (1960) used a composition from a sample from the chilled margin of the intrusion. Hoover (1989a) also used an analysis from a sample of the chilled margin but complimented it with melting experiments. Ariskin (1999) used thermodynamic modeling to make his estimates. AA1 (Fig. 43.6) is his preferred value. Nielsen (2004) based his estimate on volumes and average compositions complimented by comparison with chilled margin compositions and compositions of Tertiary basalts found near the intrusion. McBirney (1996) based his estimate on the mean composition of three samples from the chilled margin.

The estimates made by Wager (1960) and Ariskin (1999) do not fit the pattern we expect. A point representing an initial melt on a Pearce element ratio diagram should plot down-slope from the point representing our best estimate of the bulk composition of the intrusion (grey diamond, Fig. 43.6). I think it a tribute to the acumen of the estimators that all the preferred values fall close to the model line defined by the points representing the compositions of the weighted means of the major units of the intrusion.

### *43.5.2 Residual Melts*

In addition to values for the mean compositions of the rock units of the Skaergaard Intrusion and estimates of the compositions of the initial melts, there are at least two

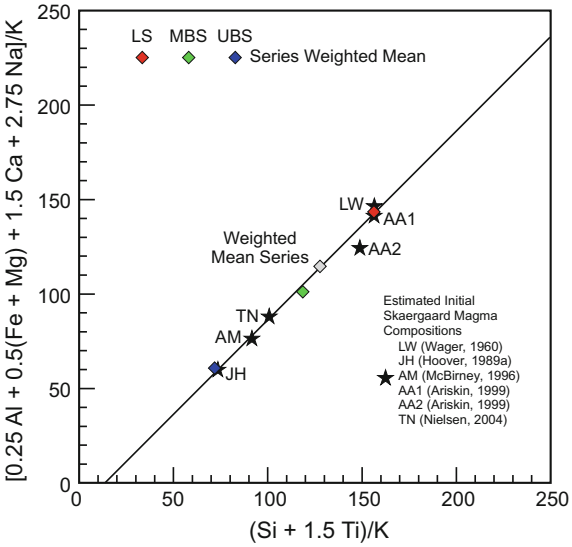


**Fig. 43.6** Pearce element ratio diagram showing the points derived from the mean compositions for Skaergaard rocks (McBirney 1996), estimates of the composition of the original Skaergaard magma (Wager 1960; Hoover 1989a, b; McBirney 1996; Nielsen 2004). The ratios plotted on the axes of the diagrams are designed such that melt and rock compositions should fall on a line with a slope of one if potassium (K) was conserved in the melts during crystallization of olivine, calcic pyroxene, plagioclase and an Fe-Ti oxide ($Usp_{75}$)

estimates of the compositions of the melt that filled the magma chamber at the time the particular crystal mush was in place: (1) experimentally determined compositions (McBirney 1996, red circles on Fig. 43.7) and (2) compositions derived through thermodynamic modeling (Ariskin 2002, green triangles on Fig. 43.7).

Felix Chayes was a petrologist who used mathematics in innovative ways to understand petrologic processes at a time when most petrologists knew little about mathematics. Among his many contributions was a small text that enhanced our understanding of the roles ratios can play in inferring petrologic processes (Chayes 1971). I met him but once at the 1967 meeting of the Geological Society of America in New Orleans. I was one of a number grad students and academics gathered in a night club. I later corresponded with him in the late 1980's about the efficacy of the correlation coefficient as a statistic for testing Pearce element ratio models. That correspondence caused me to use the designed slope of the line on a Pearce element ratio diagram as a characteristic of the model rather than a line fit to the data by least-squares methods. The designed line can then be compared to the data. Hence, one doesn't need the correlation coefficient to evaluate Pearce element ratio models. I think the same realization came independently to several others, notably Kelly Russell and Cliff Stanley, at about the same time.

In 1970 Chayes published a scheme for calculating residual melt compositions in the magma chamber and trapped in the mush during crystallization. His equation is:

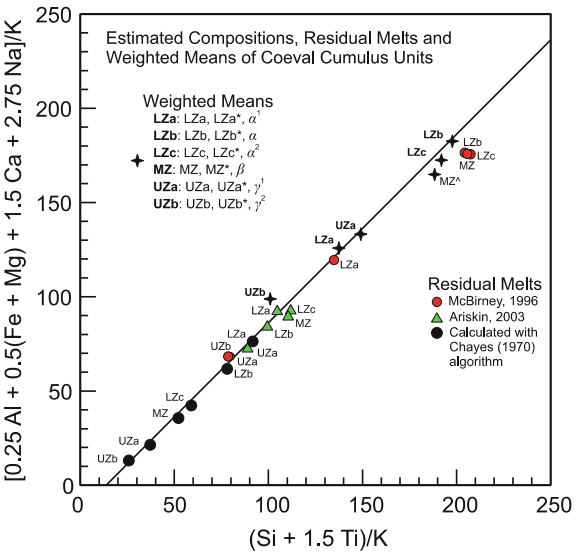


**Fig. 43.7** Pearce element ratio diagram showing the locations of points representing residual melt compositions at the end of the crystallization of the coeval units of the Skaergaard Intrusion. residual melt compositions estimated by McBirney (1996) and Ariskin (2003), and points calculated with Chayes (1970) algorithm

$$\mathbf{M}_{k+1} = \left[\mathbf{M}_1 - \sum_{j=1}^{k}\left(\mathrm{P}_j X_j\right)\right] \Big/ \left(1 - \sum_{j=1}^{k}\mathrm{P}_j\right), 0 < k < n$$

where the $\mathbf{M}_i$ are vectors whose elements are a set of oxide values in the residual melt and $n$ is the number of units in the intrusion. $\mathbf{M}_1$ is the vector containing the oxide values for the initial melt. The $P_j$ are the volumes or proportional volumes of the units in the intrusion. The $X_j$ are the mean values of the oxides in the units of the intrusion.

The values contained in the $\mathbf{M}_i$, $i > 1$, depend of the values contained in $\mathbf{M}_1$. Change the values in $\mathbf{M}_1$ and the values in $\mathbf{M}_i$ change.

All values for the initial melt, the $\mathbf{M}_1$, except those estimated by McBirney (1996) generate negative values for some of the oxides in the $\mathbf{M}_k$ at later stages in the evolution of the residual melts ($k > 3$). The Pearce element ratios for residual melts generated with Chayes' (1970) equation using McBirney's (1996) estimate for the values in the initial melt are shown with solid black circles on Fig. 43.7.

At any stage in the evolution of the Skaergaard Intrusion, the residual melt is simultaneously depositing crystals on the floor, walls and roof of the magma chamber, at least according to the simplest paradigm. The points to be compared, then, to the simulated patterns are the weighted means of the coeval units. Pearce element ratios for the three sets of residual melts: (Chayes 1970 algorithm; McBirney 1996; Ariskin 2003) can be compared on Fig. 43.7. McBirney's (1996) estimates for the compositions of the residual melts at the end of LZa, LZc, MZ, UZa, and UZb do not fit the expected pattern in that they plot up-slope from their respective cumulate compositions. All of the points representing the residual melt compositions estimated by Ariskin (2003) plot down-slope from the points

representing their respective cumulate compositions as do residual melt compositions calculated with Chayes' (1970) algorithm. Only the latter however, fall in sequential order, a pattern expected for a series of melts formed by fractionation of a single initial magma.

### 43.5.3 Relative Amounts of Trapped Melt

We can make qualitative assessments of the amount of melt trapped in the cumulates by plotting the relative volumes of the units in the intrusion against the position of the Pearce element values along the model line (see Fig. 43.2).

Data points on Pearce element ratio diagrams need not fall exactly on model lines, which makes calculating distance along the model line less straight-forward than given in the formula above (see Sect. 43.3). To calculate distance from a point representing a melt composition to a point representing a cumulate composition we measure the distance along the model line between two points that are the closest to each of the two points in question. The point of closest approach will be along a line through the point and normal to the model line. An example is shown on Fig. 43.8 for the coeval Lower Zone units (LZa, LZa*, and $\alpha^1$). The points on Fig. 43.8 represent the initial melt composition (McBirney 1996, black star) and the mean compositions of the units (McBirney 1996 coloured circles).

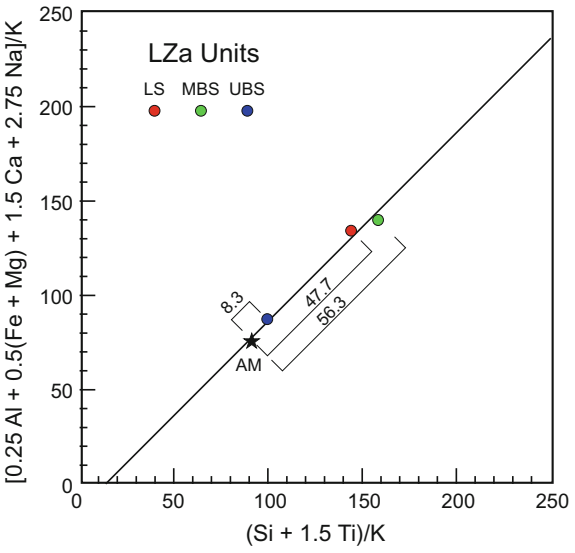


**Fig. 43.8** Pearce element ratio diagram showing distances along the model line between points representing weighted mean compositions of the LZa units and the point representing the estimate of the composition of the initial Skaergaard magma (McBirney 1996)

Figure 43.9 shows the distances along the model line versus unit size expressed as a percentage of the volume of the intrusion (Nielsen 2004). The left hand sides of the triangles defined by points representing coeval units are approximately vertical; in other words, the units whose points define the left hand sides of the triangles are approximately the same size. On Fig. 43.3, the ratio of trapped melt to primocryst in the crystal mush decreases upwards along a vertical line. If the same pattern carries over to real-world data, then the amount of trapped melt, relative to primocryst amount, is smaller in the UBS units than in the MBS units.

The lack of independence in the estimates of the volumes of the units does not in itself invalidate these conclusions. The estimates of the relative volumes may be correct; we just have less confidence that they may be. Because we are using the estimates in a qualitative fashion, the chances that our conclusions are reasonable improve.

Contours of equal trapped melt to primocryst ratio have a positive slope on Fig. 43.3, which illustrates the pattern of points in the simulation model. If the pattern applies to the real world, the upper boundaries, with negative slopes, of the triangles representing the coeval LZa and UZa units (red and yellow triangles) cannot be parallel to contours of equal ratio. We infer, then, that for these two sets of coeval units, the ratio of trapped melt to primocryst amount was smaller in the MBS units than in the LS units.

It is unlikely coeval units of the LS and the UBS would have the same ratios for trapped melt to crystals. Consequently, the lines drawn between points representing LS and UBS units are probably not lines of constant ratio (compare Fig. 43.3).

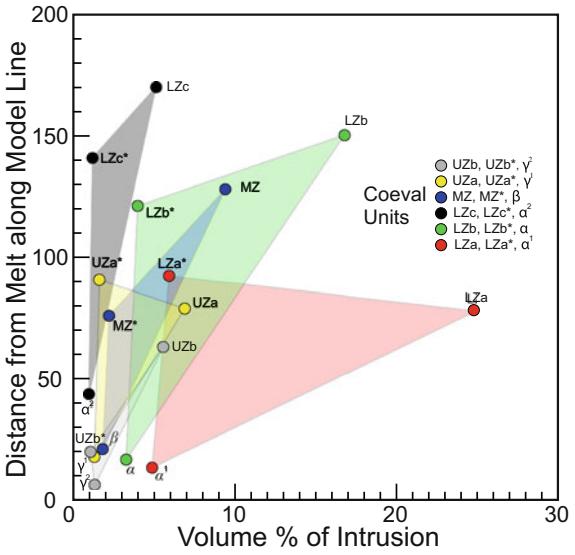


**Fig. 43.9** Distances of the locations of the points representing the compositions of coeval Skaergaard units from points representing the compositions of the residual melts (calculated with Chayes 1970, algorithm) along the model line versus the volumes of the units expressed as percentages of the volume of the intrusion (Nielsen 2004). The triangles connect vertices whose points represent properties of coeval units

## 43.6 Pearce Element Ratios, Cumulate Rocks, and September 11

Wager's discovery of the Skaergaard Intrusion and his recognition of its significance to igneous petrology and Pearce's insight that led to Pearce element ratios opened ways to decipher how cumulus rocks came to be. Understanding how these rocks came to be can affect our lives. They host ore deposits of chromium, nickel, and the platinum group elements (ruthenium, rhodium, palladium, osmium, iridium, and platinum), elements required by our civilization. To know more about how they came to be adds to our understanding of the Earth.

For nearly a decade I did little to extend the range of application of Pearce element ratios. An invitation to contribute to a review paper by *Geoscience Canada* led me to look at cumulate rocks through the lens of Pearce element ratios. Perhaps the perspective articulated by Stephen J. Gould in a piece he wrote for Canada's newspaper, the Toronto *Globe and Mail*, shortly after the events of 9/11 (Gould 2001) is apposite. His point: evil events, like 9/11, can cause big changes in our lives whereas many good events come in small packages. The good, however, by their number, eventually outweigh the evil. Maybe application of Pearce element ratios to the study of cumulate rocks can count as one of the small packages.

**Acknowledgements** Discussions with many people helped me learn about Pearce element ratios, in particular, Kelly Russell, Cliff Stanley, Terry Gordon, and Alex Wilson. Thanks to the late Tom Pearce for inventing Pearce element ratios.

## Appendix: Computer Simulation

The simulation will be for a single step or stage in the processes that lead to the development of a layered intrusion. The simulated system contains Si, Al, Mg, Ca, K, and P. Crystallization produces forsterite and anorthite with proportions of the two minerals constrained by the concentrations of Si, Al, Mg, and Ca in the melt. A fraction of the initial melt crystallizes to produce a melt modified in composition, some of which is trapped between the primocrysts.

Numbers that have to be specified to run the simulation are a composition for the initial melt (*im*[0], *im*[1], *im*[2], *im*[3], *im*[4]) where the items in the initial melt vector represent molar percentages of the elements: Si, Al, Mg, Ca, K, and P. The size (*S*) of the melt in the simulated magma chamber is entered into the simulation procedure, as is the percentage (*P*) of the initial melt, or aliquot that will supply the forsterite and anorthite crystals in the layer. The size is equal to the number of moles of the elements in the initial melt. The numbers of the different elements in the aliquot will designated as (*aq*[0], *aq*[1], *aq*[2], *aq*[3], *aq*[4], *aq*[5]).

One could assume the simulated magma chamber was initially uniformly mixed and filled with a homogeneous melt. If the composition of the system is known, the simulation could be made deterministic to within two adjustable parameters if a

thermodynamic component were included in the model. This is a consequence of Duhem's theorem (see Nicholls 1990a, 2000, 2013). One could also make it deterministic by extracting the maximum amounts of forsterite and anorthite from the aliquot. To add some variability into the simulation, we will sample the initial melt to create the aliquot by following a constrained random number procedure. $P \times S/100$ random integers, $rn$, $n = 1 \ldots P \times S/100$, are generated from a uniform distribution between 0 and $P \times S/100$.

If: $0 < rn < im[0] \times P \times S/100$,
$aq[0] = aq[0] + 1$
else if: $im[0] \times P \times S/100 < rn < im[0] \times P \times S/100 + im[1] \times P \times S/100$,
$aq[1] = aq[1] + 1$
else if: $im[0] \times P \times S/100 + im[1]\ P \times S/100 < rn <$
$im[0] \times P \times S/100 + im[1] \times P \times S/100 + im[2] \times P \times S/100$,
$aq[2] = aq[2] + 1$
else: $im[0] \times P \times S/100 + im[1] \times P \times S/100 + im[2] \times P \times S/100 < rn <$
$im[0] \times P \times S/100 + im[1] \times P \times S/100 + im[2] \times P \times S/100 + im[3] \times P \times S/100$,
$aq[3] = aq[3] + 1$
and $aq[4] = im[4] \times P \times S/100$
$aq[5] = im[5] \times P \times S/100$.

The last two equalities ensure that the two conserved elements, K and P, enter the aliquot in the same proportions as they are found in the initial melt.

From this new melt, forsterite and anorthite crystallize. The amounts of the two phases that can be extracted from the new melt are constrained by the composition of the aliquot. The amount of anorthite that can be extracted depends on the numbers of Ca and Al elements in the melt:

if: $aq[3] < aq[1]/2$,
$\mathrm{An} = aq[3]$
else $\mathrm{An} = aq[1]/2$

The amount of forsterite depends on the number of Mg elements in the melt.

$\mathrm{Fo} = aq[2]/2$

Using the amounts of anorthite and forsterite extracted from the aliquot, the numbers of elements in a new melt ($nm[0]$, $nm[1]$, $nm[2]$, $nm[3]$, $nm[4]$, $nm[5]$) are calculated by:

$nm[0] = im[0] - \mathrm{Fo} - 2\ \mathrm{An}$
$nm[1] = im[1] - 2\ \mathrm{An}$
$nm[2] = im[2] - 2\ \mathrm{Fo}$
$nm[3] = im[3] - \mathrm{An}$
$nm[4] = im[4]$
$nm[5] = im[5]$

A melt with the new composition is then trapped between crystals to form the crystal mush. Solidification of the mush produces a layer in the cumulate rock body.

## References

Anderson AT (1976) Magma mixing: petrological process and volcanological tool. J Volcanol Geotherm Res 1:3–33

Ariskin AA (1999) Phase equilibria modeling in igneous petrology: use of COMAGMAT model for simulating fractionation of ferrobasaltic magmas and the genesis of high-alumina basalt. J Volcanol Geoth Res 90:115–162

Ariskin AA (2002) Geochemical thermometry of the Layered Series rocks of the Skaergaard Intrusion. Petrol 10(6):495–518

Ariskin AA (2003) The compositional evolution of differentiated liquids from the Skaergaard Layered Series as determined by geochemical thermometry. Russ J Earth Sci 5(1):1–29

Bloss FD (1994) Crystallography and crystal chemistry. Mineralogical Society of America, Washington, DC, USA

Bons PD, Baur A, Elburg MA, Lindhuber MJ, Marks MAW, Soesoo A, van Milligen BP, Walte NP (2015) Layered intrusions and traffic jams. Geology 43(1):71–74. https://doi.org/10.1130/g36276.1

Carmichael ISE (2004) Landmark papers. Volcanic petrology. In: Wood BJ (ed) Landmark papers, vol 1. Mineralogical Society of Great Britian & Ireland, London, England, p 319

Carmichael ISE, Turner FJ, Verhoogen J (1974) Igneous petrology. McGraw-Hill Book Company, New York, USA

Cawthorn RG, Walraven F (1998) Emplacement and crystallization time for the bushveld complex. J Petrol 39(9):1669–1687

Chayes F (1956) Petrographic modal analysis an elementary statistical appraisal. Wiley, New York, USA

Chayes F (1970) On estimating the magnitude of the Hidden Zone and the compositions of the residual liquids of the Skaergaard Layered Series. J Petrol 11(1):1–14

Chayes F (1971) Ratio correlation: a manual for students of petrology and geochemistry University of Chicago Press. Illinois, USA, Chicago

Gould SJ (2001) The good people of Halifax. In: Globe and mail, Toronto, Ontario, Canada

Hoover JD (1989a) The chilled marginal gabbro and other contact rocks of the Skaegaard Intrusion. J Petrol 30(2):441–476

Hoover JD (1989b) Petrology of the marginal border series of the Skaergaard Intrusion. J Petrol 30 (2):399–439

Huppert HE, Turner JS (1981) Double-diffusive convection. J Fluid Mech 106:299–329

McBirney AR (1985) Further considerations of double-diffusive stratification and layering in the Skaergaard Intrusion. J Petrol 26(4):993–1001. https://doi.org/10.1093/petrology/26.4.993

McBirney AR (1989a) The Skaergaard Layered Series: I. Structure and average compositions. J Petrol 30:363–397

McBirney AR (1989) Geological map of the Skaergaard intrusion, east Greenland. University of Oregon, Eugene, Oregon

McBirney AR (1996) The Skaergaard Intrusion. In: Cawthorn RG (ed) Layered intrusions. Elsevier, Amsterdam, Netherlands, pp 147–180

McBirney AR, Noyes RM (1979) Crystallization and layering of the Skaergaard Intrusion. J Petrol 20(3):487–554. https://doi.org/10.1093/petrology/20.3.487

Naslund HR (1984) Petrology of the Upper Border Series of the Skaergaard Intrusion. J Petrol 25:185–212

Nicholls J (1990a) Principles of thermodynamic modeling of igneous processes. In: Nicholls J, Russell JK (eds) Modern methods of igneous petrology—understanding magmatic processes, vol Mineralogical. Society of America. Washington, D.C., pp 1–23

Nicholls J (1990b) Stochiometric constraints on variations in Pearce element ratios and analytical uncertainty in hypothesis testing. In: Russell JK, Stanley CR (eds) Theory and application of pearce element ratios to geochemical data analysis, vol 8. Geological association of Canada. Vancouver, British Columbia, pp 73–98

Nicholls J (2000) Thermodynamics of a magmatic gas phase 50 years later: comments on a paper by John Verhoogen (1949). Can Mineral 38:1313–1328
Nicholls J (2013) Perfect fractionation in multicomponent, multiphase systems. Contrib Mineral Petrol 166(3):691–701. https://doi.org/10.1007/s00410-013-0897-y
Nicholls J, Gordon TM (1994) Procedures for the calculation of axial ratios on Pearce element-ratio diagrams. Can Mineral 32:969–977
Nicholls J, Russell JK (1991) Major-element chemical discrimination of magma batches in lavas from Kilauea volcano, Hawaii, 1954–1971 eruptions. Can Mineral 29:981–993
Nicholls J, Russell JK (2016) Igneous rock associations 20. Pearce element ratio diagrams: linking geochemical data to magmatic processes. Geosci Can 43(2):133–146. http://dx.doi.org/10.12789/geocanj.2016.43.095
Nicholls J, Stout MZ (1986) Electron beam analytical instruments and the determination of modes, spatial variations of minerals and textural features of rocks in polished section. Contrib Mineral Petrol 94:395–404
Nicholls J, Stout MZ (1997) Epitactic overgrowths and intergrowths of clinopyroxene on orthopyroxene: Implications for paths of crystallization, 1881 lava flow, Mauna Loa Volcano. Hawaii Can Mineral 35:909–922
Nielsen TFD (2004) The shape and volume of the Skaergaard Intrusion, Greenland: Implications for mass balance and bulk composition. J Petrol 45(3):507–530. https://doi.org/10.1093/petrology/egg092
Pearce TH (1968) A contribution to the theory of variation diagrams. Contrib Mineral Petrol 19:142–157
Russell JK, Nicholls J (1988) Analysis of petrologic hypotheses with Pearce element ratios. Contrib Mineral Petrol 99:25–35
Sparks RSJ, Huppert HE, Kerr RC, McKenzie DP, Tait SR (1985) Postcumulus processes in layered intrusions. Geol Mag 122(5):555–568
Wager LR (1960) The major element variation of the Layered Series of the Skaergaard Intrusion and a re-estimation of the average composition of the Hidden Layered Series and of the successive residual magmas. J Petrol 1(3):364–398
Wager LR, Brown GM (1968) Layered Igneous Rocks. San Francisco, W.H, Freeman and Company
Wager LR, Deer WA (1939) Geological investigations in east Greenland. Part III. The petrology of the Skaergaard intrusion. Kangerdlugssuaq East Greenland Meddeleser om Gronland 105 (4):1–352
Wright TL, Swanson DA, Duffield WA (1975) Chemical compositions of Kilauea east-rift lava, 1968–1971. J Petrol 16:110–133